Photocatalytic Activity Enhancement for Bi_2WO_6 by Fluorine Substitution

Rui Shi, Guangli Huang, Jie Lin, and Yongfa Zhu*

Department of Chemistry, Tsinghua University, Beijing, 100084, China

Received: July 15, 2009; Revised Manuscript Received: August 31, 2009

F^- substituted Bi_2WO_6 ($Bi_2WO_{6-X}F_{2X}$) photocatalysts with high activity have been successfully synthesized by a two-step process. The effects of F^- substitution on the crystal structure and photocatalytic activity of Bi_2WO_6 were investigated. F^- substitution could change the original coordination around the W and Bi atoms. Comparing with Bi_2WO_6, the photocatalytic activity of $Bi_2WO_{6-X}F_{2X}$ increased about 2 times for degradation of MB under visible-light ($\lambda > 420$ nm) irradiation. Density functional calculations revealed that $Bi_2WO_{6-X}F_{2X}$ has a wider valence bandwidth and lower valence band position. The high activities of $Bi_2WO_{6-X}F_{2X}$ photocatalysts come from its valence band which increase the mobility of photoexcited charge carriers and possess a stronger oxidation power.

1. Introduction

In the past decades, the studies of semiconductor photocatalysts for clean hydrogen energy production and environment decontamination have attracted much interest.[1,2] Recently, some works revealed that Bi_2WO_6 could perform as an excellent photocatalytic material for water splitting and mineralization of organic pollutants under visible-light irradiation.[3−5] Its unique combination of physical and chemical properties, in terms of chemical inertness, photostability, and environmentally friendly features, make us believe it is a fine photocatalytic candidate material. Therefore, improving the photocatalytic activity of Bi_2WO_6 for practical application is significant and meaningful.

The photocatalytic activity of semiconductors is due to the production and separation of photogenerated carriers. Therefore, ways to maximize the separation efficiency and increase the oxidation power of photogenerated carriers are important in maximizing the photocatalytic efficiency. A few researchers have reported that the photocatalytic activity of semiconductor photocatalysts can be improved by surface fluorine modification or fluorine doping.[6−14] Minero et al.[6,7] studied the degradation of phenol using fluorinated TiO_2. They claimed that the enhancement effect was mainly related to the reaction of homogeneous free OH• radicals. Choi et al. investigated surface fluorination of TiO_2, and found the addition of fluoride affected not only the photodegradation rate of the pollution but also the mechanistic pathways of the pollutant degradation.[8] Hattori et al. found a significant enhancement on photocatalytic activity of TiO_2 powders or thin films by doping with F^-, and the mechanisms of photoactive enhancement were ascribed to the increase in the anatase crystallinity.[9,10] Moreover, Yu et al.[11] proposed that the doping F^- converted Ti^{4+} to Ti^{3+} by charge compensation and that the presence of a certain amount of Ti^{3+} reduced the electron−hole recombination rate.

Very recently, a few F-doped non-TiO_2 catalysts also exhibited a similar enhancement of photocatalytic activities. Fluorine interstitially doped $ZnWO_4$ has been reported recently by our group.[13] The fluorine ions could increase the coordination sphere around the W atom in a WO_6 octahedron and cause the distortion of the WO_6 octahedron in a $ZnWO_4$ crystal, resulting in an increased transfer rate of photogenerated electrons to the photocatalyst surface and the enhanced photoactivity for rhodamine B degradation. Meanwhile, fluorinated Bi_2WO_6 presented enhanced photoactivity for RhB degradation, which could be a synergetic effect of the surface fluorination and the doping of the crystal lattice.[14] On the basis of these results, it can be inferred that the introduction of fluorine, irrespective of the approaches of fluorine doping, really enhanced the photocatalytic activity of semiconductor photocatalysts.

In these cases above, the added fluorine ions are obtained by lattice fluorine doping or surface fluorination. To our knowledge, the effects of F^- substitution and heat treatment on the photocatalytic activity of Bi_2WO_6 powders have not been reported. We report herein the photocatalytic performances of F^- substituted Bi_2WO_6 ($Bi_2WO_{6-X}F_{2X}$) prepared by a two-step process. Our principal aim is to investigate the role of F^- substitution on the structure and photocatalytic activity of Bi_2WO_6. This work may provide new insights and understanding on the photocatalytic mechanisms of F^- substitution.

2. Experimental Procedures

2.1. Synthesis of Substituted Sample. $Bi_2WO_{6-X}F_{2X}$ samples were prepared by a two-step process. All chemicals used were analytic grade reagents, without further purification. The starting materials of 0.005 mol of K_2WO_4 and 15 mL of HF were stirred and heated, thus forming the $K_2WO_{4-X}F_{2X}$ compound. In what followed, the $K_2WO_{4-X}F_{2X}$ and $Bi(NO_3)_3$ were soaked in water in a stoichiometric ratio and refluxed on a mantle heater for 24 h. The products were washed with water and filtered. The obtained precursors were dried at 333 K. In order to improve the photocatalytic activity of $Bi_2WO_{6-X}F_{2X}$, the obtained samples were calcined at several temperatures for 1 h in a crucible in air. Meanwhile, Bi_2WO_6 samples were synthesized by the same method for comparison with the $Bi_2WO_{6-X}F_{2X}$ samples. $TiO_{2-X}N_X$, known for its good photocatalytic activity in decomposition of the pollutants under visible-light irradiation, was also prepared as a reference.[15]

2.2. Characterization. The purity and crystallinity of the as-prepared sample were characterized by XRD on a Bruker D8-advance diffractometer using Cu Kα radiation ($\lambda = 1.5418$ Å). The XRD data for indexing and cell-parameter calculation were collected in a scanning mode with a step length of 0.02° and a

* Corresponding author. E-mail: zhuyf@tsinghua.edu.cn. Fax: +86-10-62787601. Phone: +86-10-62787601.

10.1021/jp906680e CCC: $40.75
Published on Web 10/20/2009

preset time of 1 s/step. The ratio of Bi:W:F in the sample was determined with a sequential X-ray fluorescence spectrometer (XRF-1700, Shimazu). Raman measurements were obtained using a Renishaw RM2000 spectrometer equipped with a notch filter and a CCD detector. Diffuse reflection spectra (DRS) were obtained on a Hitachi U-3010 UV−vis spectrophotometer. Chemical characterization of the sample surface was recorded with X-ray photoelectron spectroscopy (XPS ULVAC-PHI, Quantera). The charging effect was calibrated using the binding energy of C1s.

2.3. Photocatalytic Tests and Photoelectrochemical Performance. The photocatalytic activities of the $Bi_2WO_{6-X}F_{2X}$ and Bi_2WO_6 were evaluated by degradation of MB under a 500 W Xe lamp with the 420 nm cutoff filter. The reaction cell was placed in a sealed black box of which the top was opened and the cutoff filter was placed to provide visible light irradiation. The average light intensity was 28 mW cm^{-2}. In each run, 50 mg of the $Bi_2WO_{6-X}F_{2X}$ and Bi_2WO_6 catalyst was added to 100 mL of the MB solution. After the suspension was stirred for 60 min, the light was turned on to initiate the reaction. The concentration of the MB solution was monitored using a Hitachi UV−vis spectrophotometer every 30 min. The electrochemical and photoelectric studies were performed on a CHI 660B electrochemical system (Shanghai, China) using a standard three-electrode cell with a working electrode, a platinum wire counter electrode, and a standard calomel electrode (SCE) reference electrode. The working electrodes were prepared by dip-coating: Briefly, 5 mg of photocatalyst was suspended in 3 mL of water to produce a slurry, which was then dip-coated on a 20 mm × 40 mm indium−tin oxide (ITO) glass electrode. Electrodes were exposed to UV light for 3 days to eliminate water and subsequently dried at 353 K for 2 days. All investigated working electrodes were of similar thickness (0.1−0.12 mm). Photoelectrochemical properties were measured with a 500 W Xe lamp. Unless otherwise stated, the intensity of light was 41 mW cm^{-2} with a 420 nm cutoff filter. The electrochemical impedance spectroscopy (EIS) was carried out at the open circuit potential. A sinusoidal ac perturbation of 5 mV was applied to the electrode over the frequency range 0.05−10^5 Hz. During all of the measurements, the electrolyte was 0.1 M Na_2SO_4 solution.

2.4. Calculation Method of Band Structure. In order to obtain insight into the special properties of the $Bi_2WO_{6-X}F_{2X}$, a series of first-principle calculations were performed to assess the influence of F^- on the electronic states of Bi_2WO_6. The plane-wave pseudopotential method[16,17] was used to optimize crystal geometries, to obtain the corresponding electronic band structure. In these calculations, the energy cutoff was chosen as 340 eV. The Brillouin-zone sampling was performed by using a *k*-grid of 5 × 1 × 4 points for the calculations. The generalized gradient approximation (GGA) with the Perdew, Burke, and Ernzerhof (PBE) exchange correlation functional was adopted. The presence of F atom was modeled by removing one O atom in the Bi_2WO_6 cell, thus forming the $Bi_2WO_{6-X}F_{2X}$ compound (see Figure S1 in the Supporting Information). Finally, the geometries of all of these configurations were fully optimized to an energy minimum.

3. Results and Discussion

3.1. Photocatalytic Activity Enhancement by F^- Substitution. The photoactivities of the $Bi_2WO_{6-X}F_{2X}$ and Bi_2WO_6 samples were evaluated by degradation of MB, a hazardous solution pollutant as well as a common model compound to test the photodegradation capability of photocatalysts. Figure 1 showed the relationship between calcination temperature and

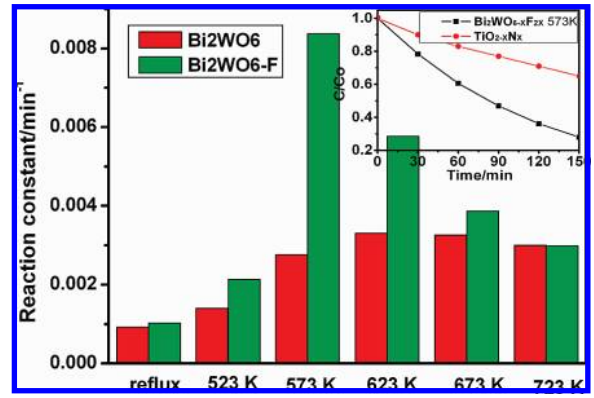

Figure 1. Photocatalytic MB degradation under visible light irradiation (λ > 420 nm) over Bi_2WO_6 and $Bi_2WO_{6-X}F_{2X}$ calcinated at several temperatures. The *X* value is the F content of $Bi_2WO_{6-X}F_{2X}$ according to XRF results. Inset: MB concentration changes over $Bi_2WO_{6-X}F_{2X}$ calcinated at 573 K and $TiO_{2-X}N_X$.

TABLE 1: Quantitative Results Give the Atomic Ratio for Bi:W:F by XRF When $Bi_2WO_{6-X}F_{2X}$ Samples Were Calcinated at Several Temperatures

	Bi	W	F
reflux	2.11	1	1.79
523 K	2.12	1	1.21
573 K	2.11	1	0.93
623 K	2.10	1	0.45
673 K	2.09	1	0.21
723 K	2.09	1	0.09

reaction constant of MB degradation over $Bi_2WO_{6-X}F_{2X}$ and Bi_2WO_6. These two samples prepared by the reflux method both showed low activities because they were not of high crystallinity and a lot of defects could act as an electron−hole recombination center. The improvement of the photocatalytic activity by calcination was due to an increase in crystallinity and a decrease in defects. Bi_2WO_6 series samples showed a similar photocatalytic activity above 573 K. $Bi_2WO_{6-X}F_{2X}$ calcined at 573 K showed the highest photocatalytic activity. It was notable that the rate of MB decomposition of $Bi_2WO_{6-X}F_{2X}$ was higher than that of Bi_2WO_6 under the same temperature treatment. Moreover, comparing with Bi_2WO_6, the photocatalytic activity of $Bi_2WO_{6-X}F_{2X}$ increased about 2 times at 573 K. The decreased activity of $Bi_2WO_{6-X}F_{2X}$ at higher calcination temperature was attributed to a decrease of F content (as shown in Table 1). When the temperature of heat treatment reached 723 K, too little F content did not influence the photocatalytic activity of $Bi_2WO_{6-X}F_{2X}$. Thus, the activity of $Bi_2WO_{6-X}F_{2X}$ was almost similar to that of Bi_2WO_6. However, calcination had some advantages, such as crystal formation and suppression of defects. In order to achieve a high photocatalytic rate, a balance between calcination temperature and F content was required. $Bi_2WO_{6-X}F_{2X}$ calcinated at 573 K (the atomic ratio for W:F was 1:0.93) gave the highest rate constant in the present work while lattice defects were suppressed and the F content was enough to influence photocatalytic activity. For comparison, the MB photodegradation by $TiO_{2-X}N_X$ was also performed. The results are shown in the inset of Figure 1. One can see that the degradation of MB over $Bi_2WO_{6-X}F_{2X}$ calcinated at 573 K was more rapid than that in the case of $TiO_{2-X}N_X$. Figure S2 in the Supporting Information showed the results of a repeated experiment for the durability of MB degradation on $Bi_2WO_{6-X}F_{2X}$. MB was quickly degraded after every injection of MB, suggesting that $Bi_2WO_{6-X}F_{2X}$ showed relatively stable performance for MB degradation. The XRD pattern was almost

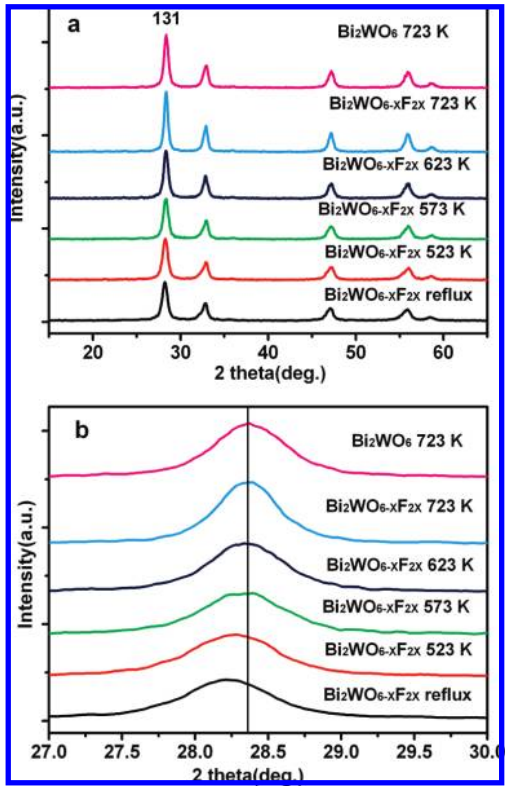

Figure 2. (a) X-ray diffraction pattern of $Bi_2WO_{6-X}F_{2X}$ calcinated at several temperatures. (b) Diffraction peak positions of the (131) plane in the range of $2\theta = 27-30°$.

similar to that of the as-prepared sample (see Figure S3 in the Supporting Information).

3.2. Effect of F^- Substitution on the Structure of Bi_2WO_6. X-ray diffraction patterns of $Bi_2WO_{6-X}F_{2X}$ obtained at different calcination temperatures were shown in Figure 2a. It illustrated that F^- substitution did not result in the development of new crystal orientations or changes in preferential orientations. Hence, independently of the presence or absence of F^-, the samples were constituted of pure orthorhombic Bi_2WO_6 phase [JCPDS No. 79-2381]. However, with the decrease in calcination temperature corresponding to an increase of F content (according to the XRF results), a comparison of the (131) diffraction peaks in the range of $2\theta = 27-30°$ (Figure 2b) showed that the peak position of $Bi_2WO_{6-X}F_{2X}$ shifted slightly toward a lower 2θ value. According to Bragg's law, the decrease in 2θ value should result in the increase in lattice parameters ($d_{(131)}$ value). Therefore, the observed shift of the diffraction peak toward lower angle could be due to the substitution of one O^{2-} by two F^- in order to maintain an electroneutrality condition. When the calcination temperature reached 723 K, the diffraction peak positions of $Bi_2WO_{6-X}F_{2X}$ and Bi_2WO_6 were the same due to the too little F content.

In order to investigate the detailed effect of F^- substitution on the structure of Bi_2WO_6, Raman patterns of $Bi_2WO_{6-X}F_{2X}$ obtained at different calcination temperatures were measured, which were shown in Figure 3. According to the XRF results as shown in Table 1, the decrease in calcination temperature corresponded to an increase of F content, which would influence the vibration mode of Bi_2WO_6. When the calcination temperature was 723 K, four main characteristic peaks of $Bi_2WO_{6-X}F_{2X}$ at 825, 793, 723, and 306 cm^{-1} can be attributed to the vibration mode of Bi_2WO_6[17] and were the same as that of Bi_2WO_6 prepared under the same synthesis conditions, which was in good agreement with XRD results. In more detail, the bands at

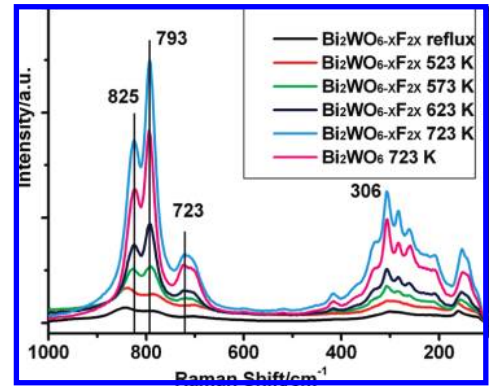

Figure 3. Raman spectroscopy of $Bi_2WO_{6-X}F_{2X}$ calcinated at several temperatures.

793 and 825 cm^{-1} are associated with antisymmetric and symmetric A_g modes of terminal O−W−O. The band at 723 cm^{-1} is interpreted as an antisymmetric bridging mode associated with the tungstate chain. The band at 306 cm^{-1} can be assigned to translational modes involving simultaneous motions of Bi^{3+} and WO_6^{6-}. As the calcination temperature decreased, the shape and location of bands of O−W−O vibration at 793 and 825 cm^{-1} were changed: the band at 793 cm^{-1} shifted to lower wavenumber, and the band at 825 cm^{-1} shifted to higher wavenumber. Moreover, the band at 723 cm^{-1} was related to vibrations of the tungstate chain, the wavenumber of which decreased with a decrease of calcination temperature. In the absence of polarization analysis, it is difficult to make an unequivocal assignment of all of the bands. However, on the basis of the above observations, the F^- substitution did influence the coordination sphere around the W atom, and the distortion of the WO_6 octahedron may exist in the $Bi_2WO_{6-X}F_{2X}$ structure.

To explore the chemical environment surrounding the W and Bi elements in $Bi_2WO_{6-X}F_{2X}$, the sample of Bi_2WO_6 was selected as a standard for XPS measurement. W4f and Bi4f X-ray photoelectron spectroscopy (XPS) results of the Bi_2WO_6 and $Bi_2WO_{6-X}F_{2X}$ samples prepared by the reflux method were shown in parts a and b of Figure 4, respectively. The binding energies of W4f5/2 and W4f7/2 are 235.9 and 232.6 eV in the oxide form of Bi_2WO_6, which could be characteristic of W species in the WO_6 octahedron. However, in the case of $Bi_2WO_{6-X}F_{2X}$, the binding energy of the peak of W4f5/2 and W4f7/2 increased about 0.3 eV, which was attributed to the change of the chemical environment surrounding W. Some mixed states such as F−W−O may be the case. Note that the same result was obtained in the binding energies of Bi4f7/2 and Bi4f5/2, which supported that F^- substitution could also influence coordination around the Bi atom. The XPS results displayed that the F^- substituted for O^{2-} in the Bi_2WO_6 cell. The binding energies of O1s and F1s could prove that the charging effect was not the reason for changing the binding energies of W4f and Bi4f between Bi_2WO_6 and $Bi_2WO_{6-X}F_{2X}$ (see Figure S4 in the Supporting Information).

3.3. Effect of F^- Substitution on Photophysical Properties and the Mechanism of Enhanced Photoactivities. DRS of the $Bi_2WO_{6-X}F_{2X}$ and Bi_2WO_6 samples are shown in Figure 5. The Bi_2WO_6 sample presented the photoabsorption ability from the UV light region to the visible light with a wavelength shorter than 460 nm, which was in good agreement with the previous report. It was noteworthy that the absorption onset of $Bi_2WO_{6-X}F_{2X}$ was red-shifted apparently. This indicated a decrease in the band gap of $Bi_2WO_{6-X}F_{2X}$. Their band gaps were calculated by the equation $\alpha h\nu = A(h\nu - E_g)^n$, in which α, ν,

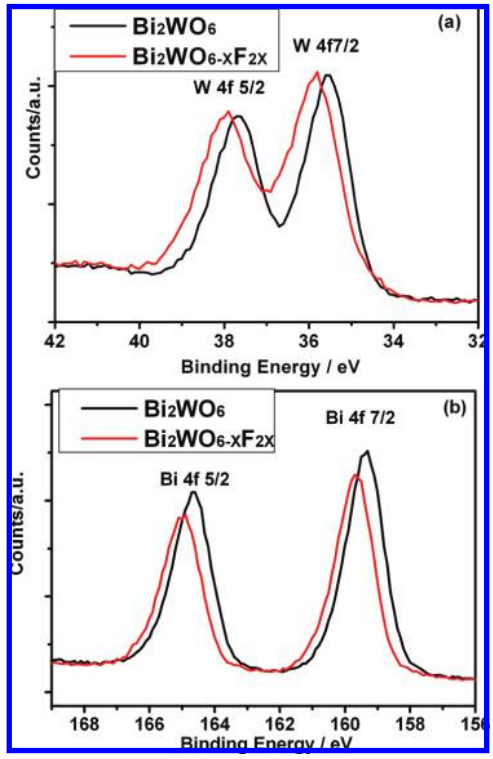

Figure 4. X-ray photoelectron spectra of Bi_2WO_6 and $Bi_2WO_{6-X}F_{2X}$ prepared by the reflux method: (a) W4f; (b) Bi4f.

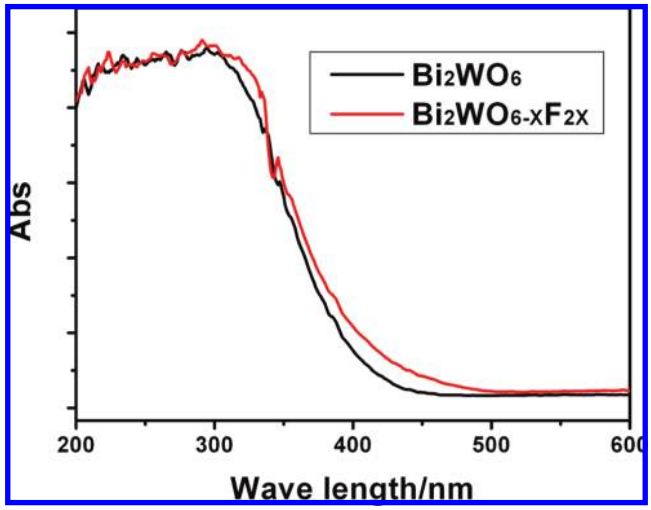

Figure 5. Diffuse reflectance spectra of Bi_2WO_6 and $Bi_2WO_{6-X}F_{2X}$ prepared by the reflux method.

A, and E_g are the absorption coefficient, light frequency, proportionality constant, and band gap, respectively (in the equation, n is decided by the characteristics of the transition in a semiconductor, here $n = 1$). Thus, the band gaps were about 2.75 and 2.64 eV for Bi_2WO_6 and $Bi_2WO_{6-X}F_{2X}$, respectively.

On the basis of XRF, XRD, Raman, and XPS results, it could be speculated that O^{2-} was substituted by F^- in the crystal lattice of Bi_2WO_6. Thus, the enhanced photoactivities could be assigned to F^- substitution. In the next section, we conducted theoretical calculations and experiments to explore the mechanism of enhanced photoactivities.

Our DFT calculations led to a band gap of 1.49 eV for Bi_2WO_6 (Figure 6a), which was smaller than the experimental value 2.75 eV. This underestimation of the band gap was due mainly to the well-known shortcoming of the exchange-correlation functional in describing excited states. For $Bi_2WO_{6-X}F_{2X}$, the band gap was calculated to be about 1.34 eV (Figure 6b). Although the band gaps calculated by the present method were usually narrower than the actual ones, the order of the calculated band gaps was the same as that experimentally determined from DRS. Thus, it was understandable that experimentally one observed a very slight decrease (about 0.11 eV) in the band gap of $Bi_2WO_{6-X}F_{2X}$.

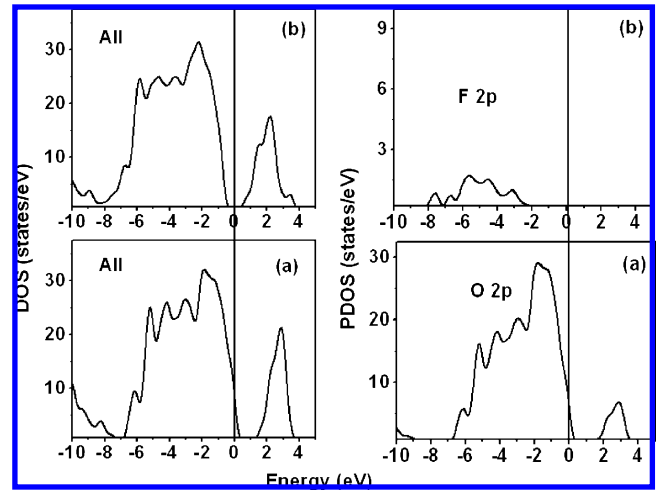

Figure 6. Total and partial DOS plots (left and right panels, respectively) calculated for (a) Bi_2WO_6 and (b) $Bi_2WO_{6-X}F_{2X}$.

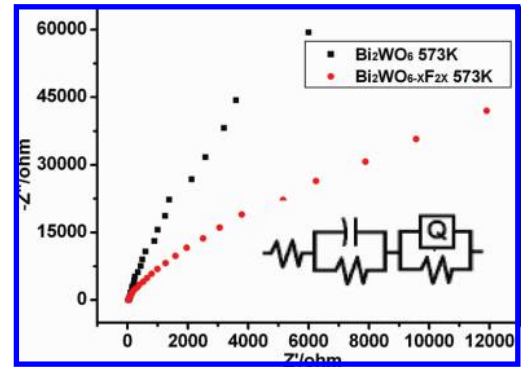

Figure 7. (a) Impedance spectra of Bi_2WO_6 and $Bi_2WO_{6-X}F_{2X}$ calcinated at 573 K electrodes under visible light ($\lambda > 420$ nm). Inset: Equivalent circuit supposed of Bi_2WO_6 and $Bi_2WO_{6-X}F_{2X}$ electrodes.

To examine the origin of the electronic structure modification of $Bi_2WO_{6-X}F_{2X}$, we calculated their partial DOS plots. The partial DOS plots presented in Figure 6b showed that most F 2p states were located in the range of the VB. The energy levels of DOS obtained by DFT calculations did not indicate the absolute values. However, we can compare the degree of dispersion of the bands of Bi_2WO_6 and $Bi_2WO_{6-X}F_{2X}$. The valence bandwidth of Bi_2WO_6 was ca. 6.5 eV. In contrast, that of $Bi_2WO_{6-X}F_{2X}$ was ca. 7.2 eV, which was wider than that of Bi_2WO_6 because the F 2p orbitals contributed to the valence band formation. Consequently, the calculation results suggested that the wider and more dispersed bands of $Bi_2WO_{6-X}F_{2X}$ would increase the mobility of photoexcited charge carriers in the valence and conduction bands.[18]

EIS could also confirm photogenerated electron−hole pairs were easier separated and transferred to the surface of the $Bi_2WO_{6-X}F_{2X}$ sample. Figure 7a showed EIS Nynquist plots of Bi_2WO_6 and $Bi_2WO_{6-X}F_{2X}$ (calcined at 573 K) electrodes under visible-light irradiation ($\lambda > 420$ nm). In our cases, only one semicircle on the EIS plane suggested charge transfer was

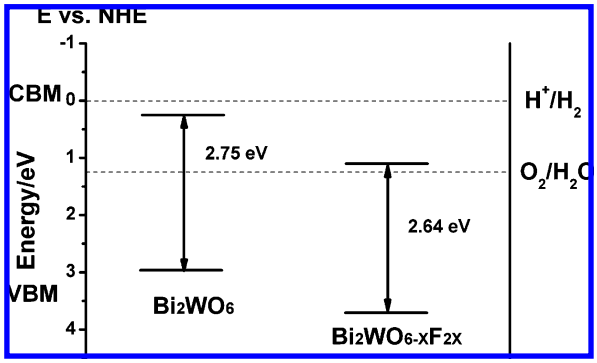

Figure 8. Comparison of the VBM and CBM positions of Bi_2WO_6 and $Bi_2WO_{6-X}F_{2X}$. The VBM and CBM values are given with respect to the normal hydrogen electrode (NHE) potential.

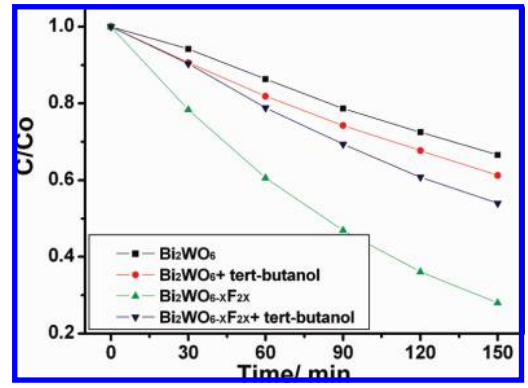

Figure 9. Effect of *tert*-butyl alcohol addition on the MB degradation over Bi_2WO_6 and $Bi_2WO_{6-X}F_{2X}$ calcinated at 573 K. [*tert*-butyl alcohol] = 1 mM.

occurring, and the supposed equivalent R(RC)(RQ) circuits are shown in the inset of Figure 7. The solution resistances of $Bi_2WO_{6-X}F_{2X}$ and Bi_2WO_6 were 30.2 and 29.7 Ω by fitting with the equivalent circuit. These two values were similar and too little comparing with the resistance of the sample, so that the difference can be neglected. The diameter of the arc radius on the EIS Nynquist plot of the $Bi_2WO_{6-X}F_{2X}$ was smaller than that of Bi_2WO_6. The smaller arc radius of the EIS Nynquist plot suggested a higher efficiency of charge separation.[19−21] Thus, in the case of $Bi_2WO_{6-X}F_{2X}$, the photoinduced electron−hole pairs were easier separated and transferred to the sample surface which was due to the wider and more dispersed valence band.

The ability of a semiconductor to photooxidate the adsorbed species on its surface is governed by the positions of its conduction band minimum (CBM) and valence band maximum (VBM) with respect to the redox potentials of the adsorbate, and thus, the photocatalytic ability of Bi_2WO_6 is determined to a great extent by the positions of its CBM and VBM.[22] To study how F^- substitution influenced the photocatalytic activity of Bi_2WO_6, we determined the CBM and VBM of unsubstituted and F^- substituted systems. The resulting VBM and CBM values were presented in Figure 8, where the VBM and CBM of Bi_2WO_6 (with respect to the normal hydrogen electrode potential) were obtained from the reference.[23] For $Bi_2WO_{6-X}F_{2X}$, the CBM were obtained from the DOS plots according to the relative positions with respect to that of Bi_2WO_6, and then the VBM were obtained from the corrected band gap. The CBM and VBM of $Bi_2WO_{6-X}F_{2X}$ were lowered from those of Bi_2WO_6 by 0.90 and 0.79 eV, respectively. The lowering of the VBM indicated that $Bi_2WO_{6-X}F_{2X}$ had a stronger oxidation power. For photooxidations occurring in oxygenated, aqueous media, the mechanism may, furthermore, involve direct reaction of the organic chemical (dye) with surface h_{vb}^+, indirect reaction with OH• radicals, or a dual mechanism involving both surface h_{vb}^+ and OH • radicals (reaction 1).

$$h_{vb}^+/OH\bullet + \text{dye(MB)} \rightarrow \text{products} \qquad (1)$$

To study the process of the photooxidation of $Bi_2WO_{6-X}F_{2X}$, experiments were carried out by adding *tert*-butyl alcohol to minimize the formation of OH• radicals. The results were shown in Figure 9. It was very interesting to see that the addition of *tert*-butyl alcohol greatly reduced the photodegradation rate of MB in the $Bi_2WO_{6-X}F_{2X}$ suspension, whereas its addition had little effect on the MB degradation in the Bi_2WO_6 suspension. This implied that the MB degradation on Bi_2WO_6 seemed to be initiated mostly by the direct surface h_{vb}^+ transfer and was hence consistent with the observation that OH• radicals could not be the main active oxygen species in the photocatalytic process of Bi_2WO_6.[24] On the other hand, a dual mechanism involving both surface h_{vb}^+ and OH• radicals was expected in the photocatalysis process of $Bi_2WO_{6-X}F_{2X}$. The different mechanism of photodegradation between Bi_2WO_6 and $Bi_2WO_{6-X}F_{2X}$ could be attributed to the stronger oxidation power of $Bi_2WO_{6-X}F_{2X}$. On the basis of the above results, the enhanced photocatalytic activity can be explained in the following way: When Bi_2WO_6 was substituted by F^-, the surface h_{vb}^+ generated in the valence band will have a stronger oxidation power. Thus, thermodynamically, OH^- (or H_2O) in the solution can easily accept a part of surface h_{vb}^+ and form OH• radicals (reaction 2) which then oxidized MB directly in the bulk solution. The higher photocatalytic oxidation rate in the $Bi_2WO_{6-X}F_{2X}$ had been ascribed to the generation of OH• radicals.

$$OH^- \text{ (or } H_2O) + h_{vb}^+ \rightarrow OH\bullet + H^+ \qquad (2)$$

4. Conclusions

A two-step process was developed for the preparation of $Bi_2WO_{6-X}F_{2X}$ photocatalysts. F^- substitution could change the original coordination around the W and Bi atoms. Comparing with Bi_2WO_6, the photocatalytic activity of $Bi_2WO_{6-X}F_{2X}$ calcinated at 573 K increased about 2 times. The enhanced photocatalytic activity came from the following: (1) the mobility of photoexcited charge carriers in the valence and conduction bands was increased. (2) $Bi_2WO_{6-X}F_{2X}$ had a stronger oxidation power, which could induce the OH• radicals to take part in the photooxidation process.

Acknowledgment. This work is supported by Chinese National Science Foundation (20925725 and 50972070) and National Basic Research Program of China (2007CB613303).

Supporting Information Available: The structure of $Bi_2WO_{6-X}F_{2X}$ used for theoretical calculations (Figure S1) and binding energies of O1s and F1s (Figure S2). This material is available free of charge via the Internet at http://pubs.acs.org.

References and Notes

(1) Asahi, R.; Morikawa, T.; Ohwaki, T.; Aoki, K.; Taga, Y. *Science* **2001**, *293*, 269.
(2) Zou, Z.; Ye, J.; Sayama, K.; Arakawa, H. *Nature* **2001**, *414*, 625.
(3) Tang, J.; Zou, Z.; Ye, J. *Catal. Lett.* **2004**, *92*, 53.

(4) Zhang, C.; Zhu, Y. *Chem. Mater.* **2005**, *17*, 3537.
(5) Fu, H.; Pan, C.; Yao, W.; Zhu, Y. *J. Phys. Chem. B* **2005**, *109*, 22432.
(6) Minero, C.; Mariella, G.; Maurino, V.; Pelizzetti, E. *Langmuir* **2000**, *16*, 2632.
(7) Minero, C.; Mariella, G.; Maurino, V.; Vione, D.; Pelizzetti, E. *Langmuir* **2000**, *16*, 8964.
(8) Vohra, M.; Kim, S.; Choi, W. *J. Photochem. Photobiol., A* **2003**, *160*, 55.
(9) Hattori, A.; Yamamoto, M.; Tada, H.; Ito, S. *Chem. Lett.* **1998**, 707.
(10) Hattori, A.; Shimoda, K.; Tada, H.; Ito, S. *Langmuir* **1999**, *15*, 5422.
(11) Yu, J. C.; Yu, J. G.; Ho, W.; Jiang, Z.; Zhang, L. *Chem. Mater.* **2002**, *14*, 3808.
(12) Li, D.; Haneda, H.; Labhsetwar, N. K.; Hishita, S.; Ohashi, N. *Chem. Phys. Lett.* **2005**, *401*, 579.
(13) Huang, G.; Zhu, Y. *J. Phys. Chem. C* **2007**, *111*, 11952.
(14) Fu, H.; Zhang, S.; Xu, T.; Zhu, Y.; Chem, J. *Environ. Sci. Technol.* **2008**, *42*, 2085.
(15) Sakthivel, S.; Janczarek, M.; Kisch, H. *J. Phys. Chem. B* **2004**, *108*, 19384.
(16) Payne, M. C.; Teter, M. P.; Allan, D. C.; Arias, T. A.; Joannopoulos, J. D. *Rev. Mod. Phys.* **1992**, *64*, 1045.
(17) Segall, M. D.; Lina, P. J. D.; Probert, M. I. J.; Pickard, C. J.; Hasnip, P. J.; Clark, S. J.; Payne, M. C. *J. Phys.: Condens. Matter* **2002**, *14*, 2717.
(18) Hosogi, Y.; Shimodaira, Y.; Kato, H.; Kobayashi, H.; Kudo, A. *Chem. Mater.* **2008**, *20*, 1299.
(19) Zhang, L.; Fu, H.; Zhu, Y. *Adv. Funct. Mater.* **2008**, *18*, 2180.
(20) Zhu, S.; Xu, T.; Fu, H.; Zhao, J.; Zhu, Y. *Environ. Sci. Technol.* **2007**, *41*, 6234.
(21) Lin, J.; Zong, R.; Zhou, M.; Zhu, Y. *Appl. Catal., B* **2009**, *89*, 425.
(22) Yang, K.; Dai, Y.; Huang, B.; Whangbo, M. *Chem. Mater.* **2008**, *20*, 6528.
(23) Fu, H.; Zhang, L.; Yao, W.; Zhu, Y. *Appl. Catal., B* **2006**, *66*, 100.
(24) Fu, H.; Pan, C.; Yao, W.; Zhu, Y. *J. Phys. Chem. B* **2005**, *109*, 22432.

JP906680E